Design and Optimization of Instability Mitigation for AC–DC Feeder Systems With Constant Power Loads Using Artificial Intelligence Techniques

Ratapon Phosung, Kongpan Areerak, *Member, IEEE*, Theppanom Sopapirm, and Kongpol Areerak, *Member, IEEE*

***Abstract*—Most electrical power system loads are actively controlled power electronics converters behaving as constant power loads. These loads resemble a small-signal negative impedance that can directly degrade the system stability margin and performance. The active damping approach is widely used for instability mitigation. However, if the mitigation is applied at the load side, it can affect the load performance. Therefore, this article presents a new design method for instability mitigation by the artificial intelligence method called the adaptive tabu search algorithm. After applying the proposed design method, the power system can maintain stable operation until achieving the rated power. Moreover, the load performance is better when the proposed design technique is applied compared to that from the conventional design. Good agreement among theoretical, simulation, and experimental results is also achieved.**

***Index Terms*—AC–DC power system, adaptive tabu search (ATS) algorithm, constant power loads (CPLs), feedforward stabilizing loop.**

I. Introduction

IT is well known that regulated power converters behave as constant power loads (CPLs) [1]–[3]. CPLs can degrade the system stability [4]–[6], resulting in huge oscillations of voltage and current responses. These oscillations may result in poor performance until the controllers fail. Most research presents the stability analysis via the averaging mathematical model with Middlebrook's criteria [7], [8] or the eigenvalue theorem [9], [10]. Analytical results can then be used to predict the unstable point and to understand the effect of parameter variation in terms of stability. In [11], for example, the analytical results obtained using the eigenvalue theorem with the averaging model show that the bandwidth of voltage loop control affects system stability. The greater the bandwidth, the less stable the system. However, if the unstable point occurs before the load is rated, the prediction from the analytical result will not allow the system to operate until the rated power is obtained. For this case, instability mitigation is required to avoid unstable operation at the rated power.

Mitigation techniques can be divided into two categories: 1) passive [12], [13] and 2) active [14]–[16]. In the passive technique, passive components are added to the system to increase system damping. The drawback of the passive method is its increase in both loss and cost. The active mitigation technique provides virtual impedance to increase system damping and can be applied to three locations. The first location is the feeder side [5], [14], [17]–[21] wherein the compensation algorithm can be applied to the controller of the feeder systems. Unfortunately, if the feeder-side system consists of uncontrolled power converters, such as a three-phase diode rectifier, the mitigation technique cannot be applied at the feeder side. The second location is the load (CPL) side [15], [22]–[29]. The mitigation signal can be injected into the control loop of the load to directly eliminate the effect of the CPL. The advantage of this technique is that it can be applied to all CPL loads. However, mitigation at the load side affects the load performance. If the feeder consists of an uncontrolled converter and the load performance is very important, the third and last location should be used. It is located between the feeder and CPL and auxiliary circuits are required [16], [30], and [31]. The drawback of this technique is that the losses and costs are increased.

Regarding the above-mentioned techniques, this article focuses on the active method at the load side for instability mitigation to avoid increasing loss and cost. The disadvantage of mitigation on the load side is that it has an impact on the load performance. Furthermore, the research on mitigation at the load side in [25]–[29] focused solely on how to eliminate the CPL effect without considering the load performance. The load performance during the mitigation controller design process has been the subject of research [22]–[24]. However, Wu *et al.* [22] considered only the simple power system without the rectifier unit, whereas in [23] and [24], the PI controllers were used to tune the resonant frequency for minimizing the effect on the load performance. These PI controller parameters are very difficult

Manuscript received August 29, 2021; revised November 12, 2021; accepted December 13, 2021. Date of publication December 17, 2021; date of current version January 19, 2022. This work was supported in part by the Suranaree University of Technology (SUT), in part by Thailand Science Research and Innovation (TSRI), and in part by the National Science, Research and Innovation Fund (NSRF) under Project 90464. Recommended for publication by Associate Editor M. Molinas. *(Corresponding author: Kongpan Areerak.)*

Ratapon Phosung, Kongpan Areerak, and Kongpol Areerak are with the School of Electrical Engineering, Institute of Engineering, Suranaree University of Technology, Nakhon Ratchasima 30000, Thailand (e-mail: ratapon@sut.ac.th; kongpan@sut.ac.th; kongpol@sut.ac.th).

Theppanom Sopapirm is with the Department of Electrical Power Engineering, Faculty of Engineering and Technology, Mahanakhon University of Technology, Bangkok 10530, Thailand (e-mail: theppanom@mutacth.com).

Color versions of one or more figures in this article are available at https://doi.org/10.1109/TPEL.2021.3136354.

Digital Object Identifier 10.1109/TPEL.2021.3136354

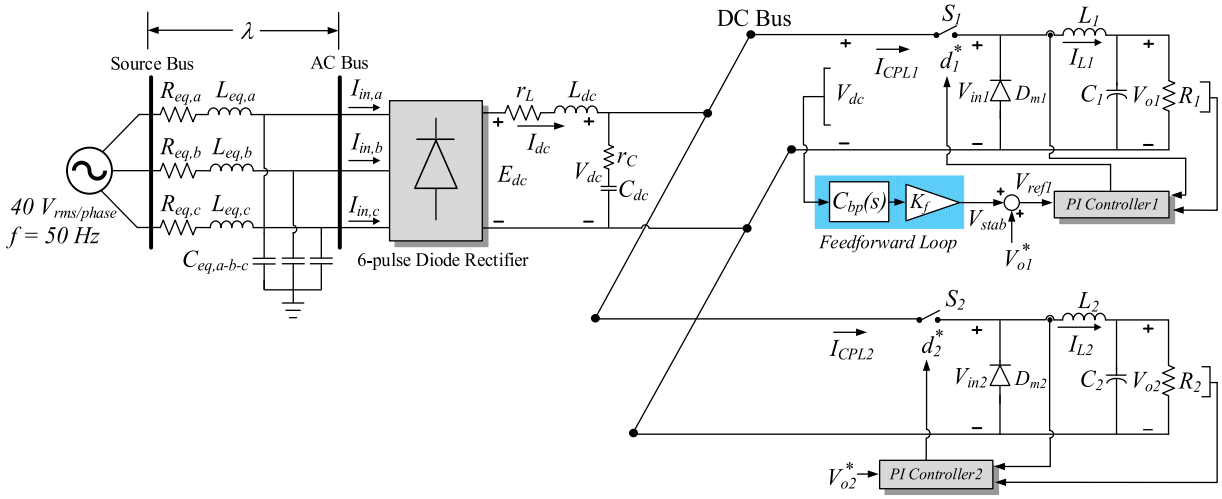

Fig. 1. AC–DC power system feeding paralleled controlled buck converters with active stabilization using a feedforward loop.

to design. Instability mitigation may fail if the appropriate PI controller is not obtained. As a result, the active method, namely the feedforward loop technique [22], [32], was used in this article to eliminate the effect of the CPL. To determine the compensated gain, as well as other feedforward loop parameters, an artificial intelligence technique known as the adaptive tabu search (ATS) algorithm [33]–[36] is used. The ATS searches gain and parameters that may affect the load performance, including those with the smallest known impact. The proposed design using AI is flexible in which other AI algorithms can be applied. The application of an artificial intelligence technique for instability mitigation has not yet been reported. The proposed mitigation technique shows that the ATS algorithm can decrease the drawback of instability mitigation located at the CPL side. After applying the proposed mitigation method, the system considered is always stable and exhibits optimal performance; the effect of the CPL is eliminated. The proposed concept of this article was validated by MATLAB simulation and by experiment. Good agreement among theoretical, simulation, and experimental results is achieved.

The rest of this article is organized as follows. The power system considered by the mathematical model for the stability analysis is introduced in Section II. The effect of CPL is also presented in Section II. In Section III, the feedforward loop is described to mitigate the instability. The ATS algorithm applied to determine the compensation gain and the feedforward parameters is addressed in Section IV. The validation of the theoretical analysis by simulation and experiments are presented in Section V. Finally, Section VI concludes this article.

II. Considered Power System With CPL Effects

The ac–dc power system considered in this study is illustrated in Fig. 1. The rated power of the proposed system was determined to be 600 W. This system can be separated into two parts. The first part is the feeder side of the dc bus in which the balanced three-phase voltage source is connected to a six-pulse diode rectifier with dc-link filters. This includes parasitic parameters (represented by r_L, $L_{\rm dc}$, r_c, and $C_{\rm dc}$) via the transmission line (represented by $R_{\rm eq}$, $L_{\rm eq}$, and $C_{\rm eq}$) to provide the power to the dc bus. The second part, called the load side, consists of controlled buck converters. The cascade PI controllers designed via the classical method in [36] were used to regulate the output dc voltage of both parallel buck converters. The system parameters of Fig. 1, without the feedforward loop, are given in the Appendix. The feedforward loop parameters designed by the proposed method in this article will be further explained in Sections III and IV.

For the case without the feedforward loop, the paralleled buck converters with controls in Fig. 1 behave as CPLs. These CPLs can degrade the system stability. Therefore, a stability study is very important. In this article, the DQ method [9], [10] was used to analyze a six-pulse diode rectifier model, whereas the generalized state-space averaging modeling approach [37] was used to derive the paralleled buck converters model. After derivation, a time-invariant model of the entire system suitable for the stability analysis by the eigenvalue theorem can be achieved. Based on the procedure in [38] and [39], the dominant eigenvalues of the system in Fig. 1 without the feedforward loop are shown in Fig. 2, with simulation and experimental validations shown in Fig. 3.

From Fig. 2 and based on the eigenvalue theorem, the system will be unstable at $P_{\rm CPL1}$ and $P_{\rm CPL2} = 160$ W (total CPL equal to 320 W). Fig. 3 shows the simulation and experimental validations of Fig. 2. It can be seen from Figs. 2 and 3 that the system becomes unstable before reaching the rated power (600 W). Therefore, the stabilization technique is required, as explained in Section III.

III. Feedforward Loop Stabilization

The proposed feedforward loop stabilization is given in Fig. 4. The feedforward loop was only used on CPL1, the first controlled buck converter. According to the literature review, mitigation on the load side can affect the load performance. As a result, the mitigation will be small enough to allow the system to operate

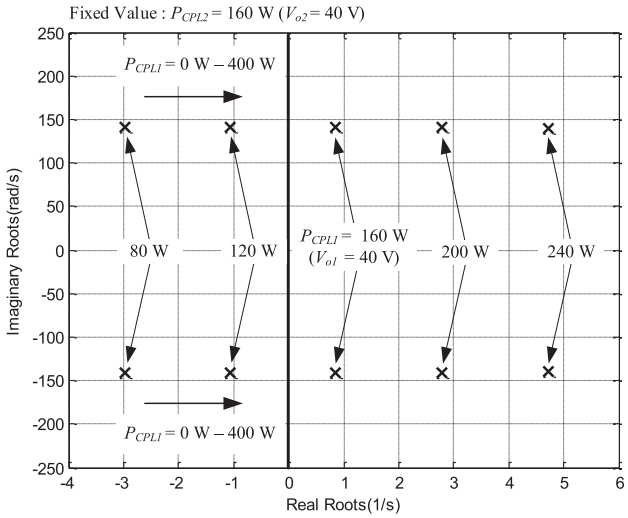

Fig. 2. Dominant eigenvalue of the system without the proposed stabilization technique.

at full power. In this article, simply connecting the feedforward loop to CPL1 is sufficient; the system can be operated at rated power ($P_{\rm CPL1} = 300$ W and $P_{\rm CPL2} = 300$ W) without unstable operation. In contrast, if only one feedforward loop mitigation is not sufficient, the instability mitigation will be applied to the second CPL2. Based on the feedforward loop stabilization, the CPL effect can be eliminated by detecting the output voltage at the dc bus ($V_{\rm dc}$). $V_{\rm dc}$ is then fed through the bandpass filter, $C_{bp}(s)$, to provide the oscillation signal (V_{bpf}) around the resonance frequency of the filter circuit (ω_r). In the steady-state condition, V_{bpf} will be equal to zero because of the derivative term within the bandpass filter. Therefore, the feedforward loop will affect only the transient response. Thereafter, V_{bpf} is scaled by multiplication with the proportional gain K_f. As a result, the compensated signal $V_{\rm stab}$ is achieved and directly injected into the control loop to generate the new voltage reference $V_{\rm ref1}$ as calculated by

$$\begin{cases} V_{\rm ref1} = V_{o1}^* + V_{\rm stab} \\ V_{\rm ref1} = V_{o1}^* + K_f \frac{(\omega_L+\omega_H)s}{s^2+(\omega_L+\omega_H)s+\omega_L\omega_H} V_{\rm dc} \end{cases} \tag{1}$$

where ω_L and ω_H are the lower and upper cutoff frequencies, respectively, and the center frequency (ω_o) can be calculated by

$$\omega_o = \sqrt{\omega_L \omega_H}. \tag{2}$$

It can be seen that there are no additional passive components or auxiliary circuits in the system when the proposed mitigation technique is applied. Only the loop control is modified so as to achieve no loss or additional cost.

From the PI controllers in the gray section of Fig. 4, the error between $V_{\rm ref1}$ and $V_{\rm o1}$ is adjusted via the control signal as expressed by

$$d_1^* = -\frac{K_{pi,1} I_{L1}}{A_{r,1}} - \frac{K_{pv,1} K_{pi,1} V_{o1}}{A_{r,1}} + \frac{K_{iv,1} K_{pi,1} X_{v1}}{A_{r,1}} + \frac{K_{ii,1} X_{i1}}{A_{r,1}} + \frac{K_{pv,1} K_{pi,1} V_{o1}^*}{A_{r,1}} + \frac{K_{pv,1} K_{pi,1} K_f V_{bpf}}{A_{r,1}} \tag{3}$$

until it is equal to zero. As a consequence, V_{o1} will be tightly controlled to track $V_{\rm ref1}$.

According to (1) and (3), an appropriately compensated gain (K_f), including the filter frequency ω_L, ω_H, and ω_o, must be designed. In this article, a design based on the proposed dynamic model with the eigenvalue theorem, called the conventional design method, is first introduced in Section III. The proposed optimal design using the ATS algorithm will then be demonstrated in Section IV. The mitigated system is expected to be stable within the rated power (600 W). The details of the design of the gain and filter frequencies are described as follows.

A. Conventional Design Method

The bandpass filter can be designed via the approach in [22] and [32] in which the center frequency ω_o is designed equally to the resonance frequency ω_r. As for the cutoff frequency, ω_H is defined to be two times the resonance frequency ($2\omega_r$), whereas ω_L is defined to be $0.5\omega_r$. For the power system with parameters listed in the appendix, ω_L and ω_H are equal to 71.64 and 286.57 rad/s, respectively.

K_f depends on the power level of the CPLs. Therefore, the proposed averaging model was used with the eigenvalue theorem to provide the appropriate K_f for stable operation. Details on how to derive the dynamic model can be found in [38]. The averaging mathematical model of the proposed ac–dc power system feeding the paralleled buck converters with the feedforward stabilizing loop shown in Fig. 1 is given by the following equation (16 state variables): (4) shown at the next page.

The dynamic model of (4) was linearized by the first-order term of the Taylor series. The linearized model of (4) was then used with the eigenvalue theorem with the system parameters from the appendix and with the CPL fixed to the rated power of 600 W. The resulting dominant eigenvalue plot, when the gain K_f was varied from zero to five, is shown in Fig. 5. It can be seen from the trajectory of the eigenvalue in Fig. 5 that the dominant eigenvalues (in black) are located at the right-hand side when K_f ranges from 0 to 0.25. This means that the system becomes unstable at $P_{\rm CPL} = 600$ W if $K_f \leq 0.25$.

Fortunately, the system will operate stably again when $0.5 \leq K_f \leq 5$. To confirm the analytical results, intensive time-domain simulations were performed when the feedforward loop was activated with $K_f = 0.5$ and $K_f = 5$, as given in Fig. 6. It can be seen from Fig. 6 that $P_{\rm CPL,Total}$ was initially set to 320 W ($P_{\rm CPL1} = 20$ W and $P_{\rm CPL2} = 300$ W). At the initial state, the system should be unstable at $P_{\rm CPL,Total} = 320$ W without the proposed mitigation technique, as already investigated in Figs. 2 and 3. When the proposed mitigation was applied, the system was stable, as shown in the initial state of Fig. 6. At $t = 2.5$ s, $P_{\rm CPL1}$ increased to 300 W. As a result, $P_{\rm CPL,Total}$ becomes 600 W (rated power). At the rated power, the system can remain stable following the theoretical result of Fig. 5. Moreover, it is indicated that a larger K_f can generate a greater stability

margin. Less oscillation of the output voltage at the dc bus can be achieved when K_f is increased.

Focusing on the load performance, it can be observed from the zoomed area of Fig. 6 that when $K_f = 5.0$, the V_{o1} response has a larger overvoltage compared with the V_{o1} response for $K_f = 0.5$. Based on the conventional design, K_f should be sufficiently small to avoid the load performance effect. It can be seen from Fig. 6 that the mitigation approach at the load side can affect the load performance. The design of K_f is very important. In this article, the ATS algorithm is used to overcome this problem. The minimization of the load performance effect when the proposed feedforward loop is applied will be explained in Section IV.

Furthermore, it can be seen from Fig. 5 that when K_f is increased, the dominant eigenvalues are changed from the black poles to the red poles. To identify the contribution of the state-variable as well as system parameters, the participation matrix [calculated from the proposed model of (4)] for without mitigation ($K_f = 0$), lightly mitigation ($K_f = 0.5$), and highly mitigation ($K_f = 5.0$) are given in Tables IV, V, and VI, respectively (see Appendix). The condition for selecting the dominant mode of the participation matrix is that if any eigenvalue $\lambda_k = \sigma_k \pm j\omega_k$

$$
\begin{cases}
\dot{I}_{sd} = -\frac{R_{\rm eq}}{L_{\rm eq}} I_{sd} + \omega I_{sq} - \frac{1}{L_{\rm eq}} V_{{\rm bus},d} + \frac{1}{L_{\rm eq}} \sqrt{\frac{3}{2}} V_m \cos(\lambda) \\
\dot{I}_{sq} = -\omega I_{sd} - \frac{R_{\rm eq}}{L_{\rm eq}} I_{sq} - \frac{1}{L_{\rm eq}} V_{{\rm bus},q} + \frac{1}{L_{\rm eq}} \sqrt{\frac{3}{2}} V_m \sin(\lambda) \\
\dot{V}_{{\rm bus},d} = \frac{1}{C_{\rm eq}} I_{sd} + \omega V_{bus,q} - \sqrt{\frac{3}{2}} \frac{2\sqrt{3}}{\pi C_{eq}} I_{dc} \\
\dot{V}_{{\rm bus},q} = -\omega V_{{\rm bus},d} + \frac{1}{C_{\rm eq}} I_{sq} \\
\dot{I}_{\rm dc} = \sqrt{\frac{3}{2}} \frac{2\sqrt{3}}{\pi L_{\rm dc}} V_{{\rm bus},d} - \frac{(r_\mu + r_L + r_c)}{L_{\rm dc}} I_{\rm dc} - \frac{1}{L_{\rm dc}} V_{\rm dc} \\
\quad - \frac{r_c K_{pi,1}}{A_{r,1} L_{\rm dc}} {I_{L1}}^2 - \frac{r_c K_{pv,1} K_{pi,1}}{A_{r,1} L_{\rm dc}} I_{L1} V_{o1} + \frac{r_c K_{iv,1} K_{pi,1}}{A_{r,1} L_{\rm dc}} I_{L1} X_{v1} \\
\quad + \frac{r_c K_{ii,1}}{A_{r,1} L_{\rm dc}} I_{L1} X_{i1} + \frac{r_c K_{pv,1} K_{pi,1}}{A_{r,1} L_{\rm dc}} I_{L1} {V_{o1}}^* \\
\quad + \frac{r_c K_{pv,1} K_{pi,1} K_f}{A_{r,1} L_{\rm dc}} I_{L1} V_{bpf} - \frac{r_c K_{pi,2}}{A_{r,2} L_{\rm dc}} {I_{L2}}^2 \\
\quad - \frac{r_c K_{pv,2} K_{pi,2}}{A_{r,2} L_{\rm dc}} I_{L2} V_{o2} + \frac{r_c K_{iv,2} K_{pi,2}}{A_{r,2} L_{\rm dc}} I_{L2} X_{v2} \\
\quad + \frac{r_c K_{ii,2}}{A_{r,2} L_{\rm dc}} I_{L2} X_{i2} + \frac{r_c K_{pv,2} K_{pi,2}}{A_{r,2} L_{\rm dc}} I_{L2} {V_{o2}}^* \\
\dot{V}_{\rm dc} = \frac{1}{C_{\rm dc}} I_{\rm dc} + \frac{K_{pi,1}}{A_{r,1} C_{\rm dc}} {I_{L1}}^2 + \frac{K_{pv,1} K_{pi,1}}{A_{r,1} C_{\rm dc}} I_{L1} V_{o1} \\
\quad - \frac{K_{iv,1} K_{pi,1}}{A_{r,1} C_{\rm dc}} I_{L1} X_{v1} - \frac{K_{ii,1}}{A_{r,1} C_{\rm dc}} I_{L1} X_{i1} - \frac{K_{pv,1} K_{pi,1}}{A_{r,1} C_{\rm dc}} I_{L1} {V_{o1}}^* \\
\quad - \frac{K_{pv,1} K_{pi,1} K_f}{A_{r,1} C_{\rm dc}} I_{L1} V_{bpf} + \frac{K_{pi,2}}{A_{r,2} C_{\rm dc}} {I_{L2}}^2 + \frac{K_{pv,2} K_{pi,2}}{A_{r,2} C_{\rm dc}} I_{L2} V_{o2} \\
\quad - \frac{K_{iv,2} K_{pi,2}}{A_{r,2} C_{\rm dc}} I_{L2} X_{v2} - \frac{K_{ii,2}}{A_{r,2} C_{\rm dc}} I_{L2} X_{i2} - \frac{K_{pv,2} K_{pi,2}}{A_{r,2} C_{\rm dc}} I_{L2} {V_{o2}}^* \\
\dot{I}_{L1} = -\frac{K_{pi,1}}{A_{r,1} L_1} V_{\rm dc} I_{L1} - \frac{K_{pv,1} K_{pi,1}}{A_{r,1} L_1} V_{\rm dc} V_{o1} - \frac{1}{L_1} V_{o1} \\
\quad + \frac{K_{iv,1} K_{pi,1}}{A_{r,1} L_1} V_{\rm dc} X_{v1} + \frac{K_{ii,1}}{A_{r,1} L_1} V_{\rm dc} X_{i1} \\
\quad + \frac{K_{pv,1} K_{pi,1}}{A_{r,1} L_1} V_{\rm dc} {V_{o1}}^* - \frac{K_{pv,1} K_{pi,1} K_f}{A_{r,1} L_1} V_{\rm dc} V_{bpf} \\
\dot{V}_{o1} = \frac{1}{C_1} I_{L1} - \frac{1}{R_1 C_1} V_{o1} \\
\dot{X}_{v1} = -V_{o1} + {V_{o1}}^* + K_f V_{bpf} \\
\dot{X}_{i1} = -I_{L1} - K_{pv,1} V_{o1} + K_{iv,1} X_{v,1} + K_{pv,1} {V_{o1}}^* + K_{pv,1} K_f V_{bpf} \\
\dot{V}_{df} = V_{bpf} \\
\dot{V}_{bpf} = (\omega_L + \omega_H) V_{\rm dc} - \omega_L \omega_H V_{df} - (\omega_L + \omega_H) V_{bpf} \\
\dot{I}_{L2} = -\frac{K_{pi,2}}{A_{r,2} L_2} V_{\rm dc} I_{L2} - \frac{K_{pv,2} K_{pi,2}}{A_{r,2} L_2} V_{\rm dc} V_{o2} \\
\quad - \frac{1}{L_2} V_{o2} + \frac{K_{iv,2} K_{pi,2}}{A_{r,2} L_2} V_{\rm dc} X_{v2} \\
\quad + \frac{K_{ii,2}}{A_{r,2} L_2} V_{\rm dc} X_{i2} + \frac{K_{pv,2} K_{pi,2}}{A_{r,2} L_2} V_{\rm dc} {V_{o2}}^* \\
\dot{V}_{o2} = \frac{1}{C_2} I_{L2} - \frac{1}{R_2 C_2} V_{o2} \\
\dot{X}_{v2} = -V_{o2} + {V_{o2}}^* \\
\dot{X}_{i2} = -I_{L2} - K_{pv,2} V_{o2} + K_{iv,2} X_{v,2} + K_{pv,2} {V_{o2}}^*
\end{cases}
\tag{4}
$$

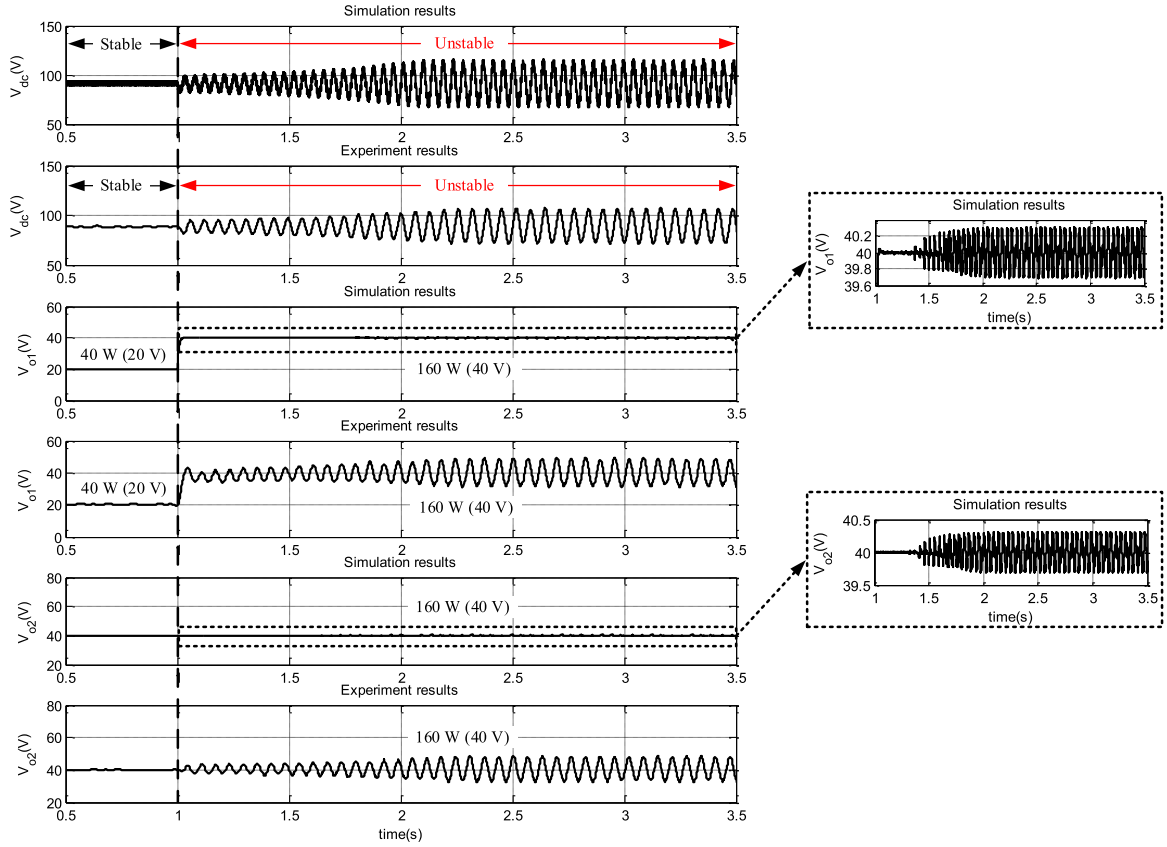

Fig. 3. Simulation and experimental validations of Fig. 2.

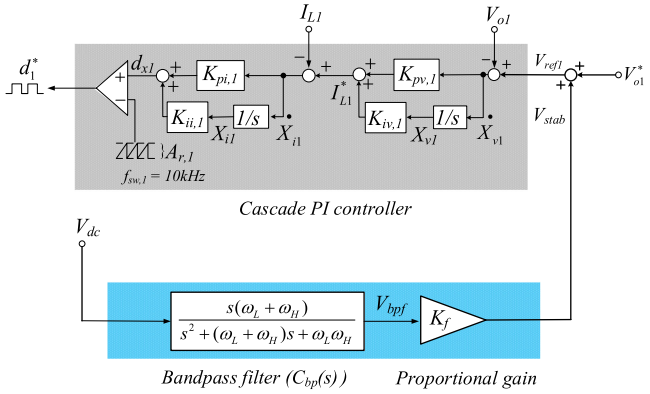

Fig. 4. Cascade PI controllers modified by the feedforward loop.

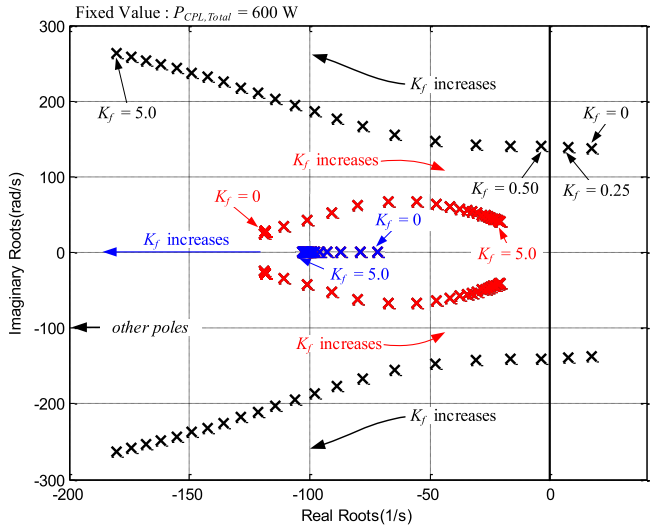

Fig. 5. Dominant eigenvalue plot for the ac–dc power system feeding CPLs with a feedforward loop designed by the conventional method.

has $|\sigma_k|<\varepsilon$ (closed to the imaginary axis), or $\sigma_k > 0$ (unstable pole), then this is a dominant mode at that operating condition.

From Table IV (without mitigation case) and Table V (lightly mitigation case), it can be observed that the state-variables $I_{\rm dc}$ and $V_{\rm dc}$ participate most heavily in the dominant modes. As a result, $I_{\rm dc}$ and $V_{\rm dc}$ will be related to the black dominant poles in Fig. 5. In Table VI (highly mitigated case), the state-variables $I_{\rm dc}$ and V_{df} play the most important roles in the dominant modes. As a result, $I_{\rm dc}$ and V_{df} will be related to the red dominant poles in Fig. 5. It can be concluded that $L_{\rm dc}$ and $C_{\rm dc}$ (related to state-variables $I_{\rm dc}$ and $V_{\rm dc}$) are significant for the cases of without mitigation and lightly mitigation. The oscillation frequency of the system response as well as the location of the dominant poles depends on the parameters $L_{\rm dc}$ and $C_{\rm dc}$. In contrast, for the high mitigation, $L_{\rm dc}$ is still the main contribution. However, ω_H and ω_L of the bandpass filter become more important than $C_{\rm dc}$. As a result, for the high mitigation case, $L_{\rm dc}$ and bandpass

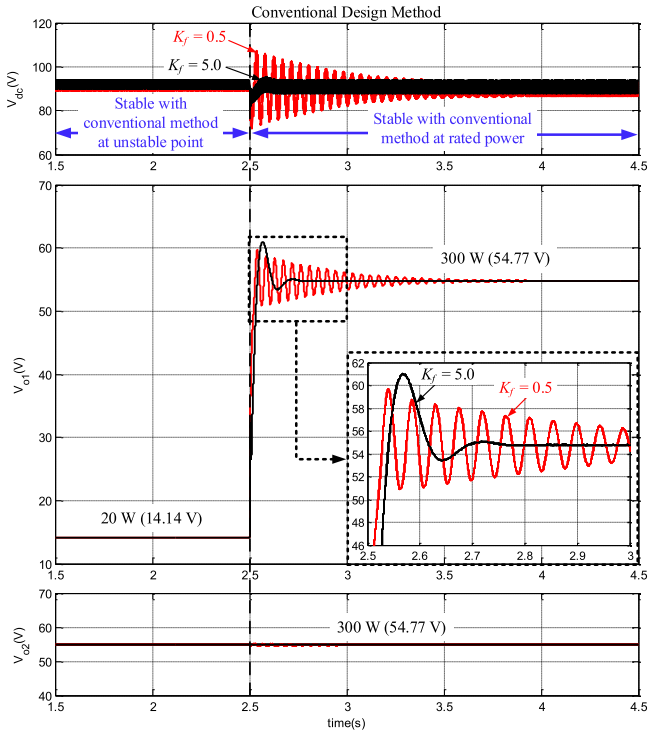

Fig. 6. Time-domain simulation results for investigating the efficiency of the conventional design.

TABLE I
COMPARISON RESULTS BETWEEN THE CONVENTIONAL DESIGN METHOD AND ATS DESIGN METHOD

Feedforward loop parameters/W value	Design method	
	Conventional method	ATS method
K_f	0.5	2.9001
ω_L (rad/s)	71.64	21.7401
ω_H (rad/s)	286.57	429.8605
W	1.0	0.6471

TABLE II
PERFORMANCE COMPARISON OF V_{o1} FROM THE SIMULATION RESULTS AT THE RATED POWER OF FIG. 16

Performance Index	Design method	
	Conventional method	ATS method
T_r (s)	0.0236	0.0373
T_s (s)	0.3752	0.1415
$P.O.$ (%)	2.3192	0.3107

filter parameters are important in determining the oscillation frequency of the system response.

IV. OPTIMAL FEEDFORWARD LOOP DESIGN

In this section, a new methodology for designing the feedforward loop is introduced. The ATS is selected for the optimal design because it was proven in [33] that this algorithm can provide the convergence property and capability to escape the local solution.

TABLE III
PERFORMANCE COMPARISON OF V_{o1} FROM THE EXPERIMENTAL RESULTS AT THE RATED POWER OF FIG. 16

Performance Index	Design method	
	Conventional method	ATS method
T_r (s)	0.0397	0.0457
T_s (s)	0.4967	0.1087
$P.O.$ (%)	4.5227	2.8455

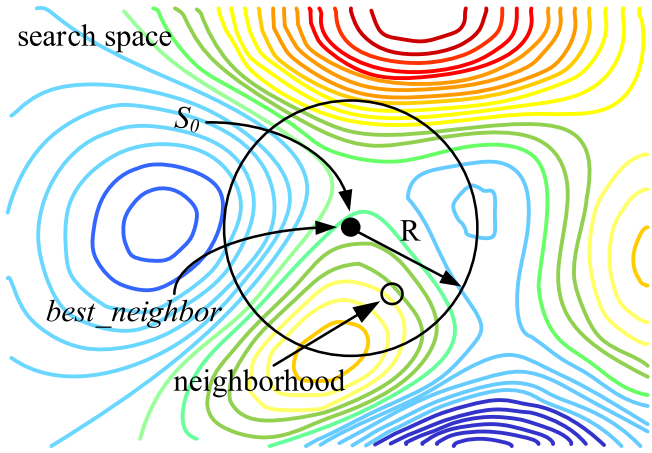

Fig. 7. Random S_0 in search space.

A. ATS Algorithm

The ATS algorithm is improved from the tabu search (TS) method by adding two mechanisms namely back-tracking and adaptive search radius. The modified version of the TS method has been named the adaptive tabu search of ATS.

The ATS algorithm can be outlined as follows.

Step 1: Initialize the tabu list TL, and Count (several searches round) = 0.

Step 2: Randomly select the initial solution S_0 from the search space. S_0 is set as a local minimum and S_0 = best_neighbor as shown in Fig. 7.

Step 3: Update *Count*, then randomly select N new solutions from the search space of a radius R. Let $S_1(r)$ be a set containing N solutions as shown in Fig. 8.

Step 4: Compute the cost value of each member of $S_1(r)$. Then, choose the best solution and assign it as best_neighbor1 (see Fig. 8).

Step 5: If *best_neighbor1* < *best_neighbor*, then keep best_neighbor in the *TL*, set *best_neighbor* = *best_neighbor1* (see Fig. 9), and set S_0 = *best_neighbor* (see Fig. 10). Otherwise, put *best_neighbor1* in the *TL* instead.

Step 6: Evaluate the termination criteria and the aspiration criteria. If Count ≥ MAX_Count (the maximum number allowance of search round), stop the searching process. The best solution available right now is the best solution overall. Otherwise, return to Step 2 and repeat the search until all of the conditions are met (see Fig. 11).

Back-tracking allows the system to go back in time and look up previous solutions in TL. The better solution is then selected

TABLE IV
PARTICIPATION MATRIX FOR WITHOUT MITIGATION CASE

	Eig. I	Eig. II	Eig. III	⋯	**Eig. VII**	**Eig. VIII**	⋯	Eig. XIV	Eig. XV	Eig. XVI
I_{sd}	0.4935	0.4935	0.0007	⋯	0.0060	0.0060	⋯	1.3×10^{-33}	1.8×10^{-30}	1.8×10^{-30}
I_{sq}	7.2×10^{-4}	7.2×10^{-4}	0.4993	⋯	2.1×10^{-17}	2.1×10^{-17}	⋯	4.8×10^{-47}	2.9×10^{-46}	2.9×10^{-46}
⋮	⋮	⋮	⋮		⋮	⋮		⋮	⋮	⋮
$\boldsymbol{I_{dc}}$	0.0060	0.0060	8.4×10^{-6}	⋯	**0.5149**	**0.5149**	⋯	1.1×10^{-31}	1.6×10^{-28}	1.6×10^{-28}
$\boldsymbol{V_{dc}}$	5.8×10^{-11}	5.8×10^{-11}	8.6×10^{-14}	⋯	**0.5103**	**0.5103**	⋯	8.9×10^{-18}	6.2×10^{-29}	6.2×10^{-29}
⋮	⋮	⋮	⋮		⋮	⋮		⋮	⋮	⋮
V_{df}	5.4×10^{-34}	5.4×10^{-34}	7.9×10^{-37}	⋯	4.3×10^{-17}	4.3×10^{-17}	⋯	2.9×10^{-33}	1.6×10^{-30}	1.6×10^{-30}
⋮	⋮	⋮	⋮		⋮	⋮		⋮	⋮	⋮
X_{i2}	8.5×10^{-19}	8.5×10^{-19}	1.3×10^{-21}	⋯	0.0054	0.0054	⋯	0.2924	0.0614	0.0614
	Mode I		Mode II	⋯	**Mode IV (Dominant mode)**		⋯	Mode VIII	Mode IX	

TABLE V
PARTICIPATION MATRIX FOR LIGHTLY MITIGATION CASE

	Eig. I	Eig. II	Eig. III	⋯	**Eig. VII**	**Eig. VIII**	⋯	Eig. XIV	Eig. XV	Eig. XVI
I_{sd}	0.4935	0.4935	0.0007	⋯	0.0064	0.0064	⋯	2.2×10^{-32}	1.4×10^{-31}	1.3×10^{-31}
I_{sq}	0.0007	0.0007	0.4993	⋯	2.1×10^{-17}	2.1×10^{-17}	⋯	2.1×10^{-45}	4.6×10^{-46}	4.6×10^{-46}
⋮	⋮	⋮	⋮		⋮	⋮		⋮	⋮	⋮
$\boldsymbol{I_{dc}}$	0.0057	0.0057	8.4×10^{-6}	⋯	**0.5514**	**0.5514**	⋯	1.9×10^{-30}	1.2×10^{-29}	1.1×10^{-29}
$\boldsymbol{V_{dc}}$	5.8×10^{-11}	5.8×10^{-11}	8.6×10^{-14}	⋯	**0.5459**	**0.5459**	⋯	1.7×10^{-29}	1.2×10^{-29}	1.2×10^{-29}
⋮	⋮	⋮	⋮		⋮	⋮		⋮	⋮	⋮
V_{df}	9.1×10^{-24}	9.1×10^{-24}	1.4×10^{-26}	⋯	0.0700	0.0700	⋯	1.1×10^{-17}	1.2×10^{-15}	1.2×10^{-15}
⋮	⋮	⋮	⋮		⋮	⋮		⋮	⋮	⋮
X_{i2}	8.5×10^{-19}	8.5×10^{-19}	1.3×10^{-21}	⋯	0.0065	0.00658	⋯	0.1626	0.1277	0.1277
	Mode I		Mode II	⋯	**Mode IV (Dominant mode)**		⋯	Mode VIII	Mode IX	

from the current and previous solutions. The back-tracking process is depicted in detail in Fig. 12.

Given this new search space to explore, the search process is likely to have more chances of escaping from the local optimum. The back-tracking mechanism can be added into Step 5 to improve the searching performance.

During the searching process, the adaptive radius process, depicted in Fig. 13, reduces the search area. The adaptive radius

TABLE VI
PARTICIPATION MATRIX FOR HIGHLY MITIGATION CASE

	Eig. I	Eig. II	Eig. III	⋯	**Eig. X**	**Eig. XI**	⋯	Eig. XIV	Eig. XV	Eig. XVI
I_{sd}	0.4935	0.4935	0.0007	⋯	0.0064	0.0064	⋯	3.5×10^{-33}	1.5×10^{-31}	1.5×10^{-31}
I_{sq}	0.0007	0.0007	0.4993	⋯	6.8×10^{-18}	6.8×10^{-18}	⋯	1.7×10^{-44}	8.6×10^{-46}	8.7×10^{-46}
⋮	⋮	⋮	⋮		⋮	⋮		⋮	⋮	⋮
$\boldsymbol{I_{dc}}$	0.0057	0.0057	8.4×10^{-6}	⋯	**0.5455**	**0.5455**	⋯	3.0×10^{-31}	1.3×10^{-29}	1.3×10^{-29}
V_{dc}	5.8×10^{-11}	5.8×10^{-11}	8.6×10^{-14}	⋯	0.0474	0.0474	⋯	3.2×10^{-30}	6.3×10^{-30}	6.4×10^{-30}
⋮	⋮	⋮	⋮		⋮	⋮		⋮	⋮	⋮
$\boldsymbol{V_{df}}$	9.1×10^{-23}	9.1×10^{-23}	1.4×10^{-25}	⋯	**0.5736**	**0.5736**	⋯	6.0×10^{-18}	2.4×10^{-17}	2.4×10^{-17}
⋮	⋮	⋮	⋮		⋮	⋮		⋮	⋮	⋮
X_{i2}	8.5×10^{-19}	8.5×10^{-19}	1.3×10^{-21}	⋯	0.0004	0.0004	⋯	0.6740	0.1233	0.1233
	Mode I		Mode II	⋯	**Mode VI (Dominant mode)**		⋯	Mode VIII	Mode IX	

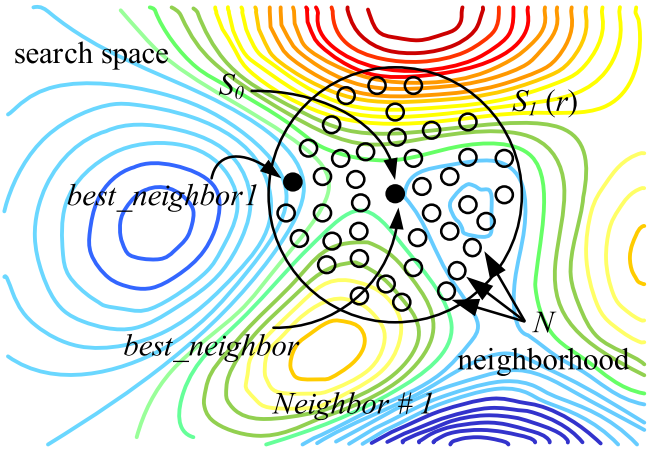

Fig. 8. Neighborhood around S_0.

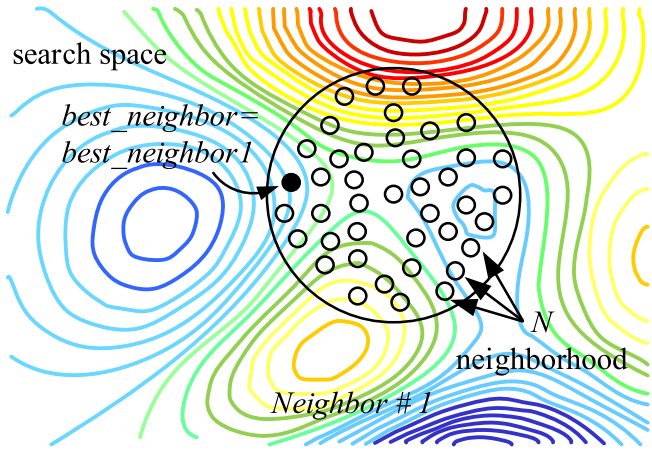

Fig. 9 Assign a new best_neighbor.

mechanism was formed to adjust the radius (R) based on the cost of the solution. The criterion for adapting the search radius is given in

$$\text{radius}_{\text{new}} = \frac{\text{radius}_{\text{old}}}{\text{DF}} \tag{5}$$

where DF is a decreasing factor. The adaptive search radius mechanism can be added to the end of Step 6 to improve the searching performance.

The ATS will search the feedforward parameters (K_f, ω_L, and ω_H) until the optimal solution can be achieved, resulting in the minimum load performance effect. A block diagram for the optimal feedforward loop design by the ATS algorithm is shown in Fig. 14. The stability analysis via the proposed dynamic model with the eigenvalue theorem was used as the penalty condition during the search process.

The details of the design process are explained as follows.

Step 1: Define the P_{CPL1} via the command input V_{o1}^*. In this article, P_{CPL2} is always set to 300 W (rated power of the second buck converter). There are the following four conditions for setting P_{CPL1}:

Condition 1: Changing P_{CPL1} from 20 W to 100 W;
Condition 2: Changing P_{CPL1} from 100 W to 180 W;
Condition 3: Changing P_{CPL1} from 180 W to 240 W;

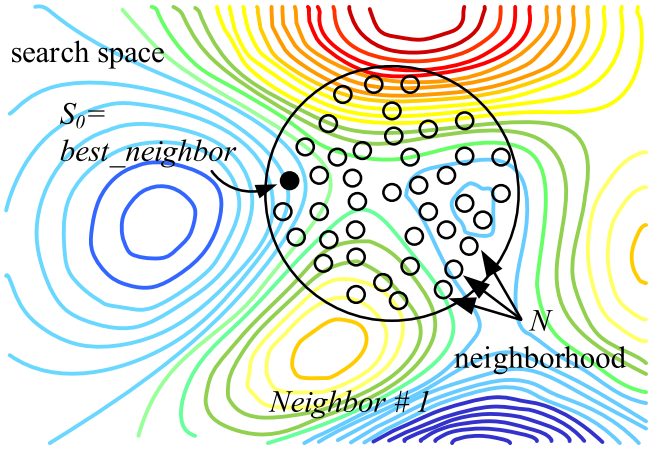

Fig. 10. Assign a new S_0.

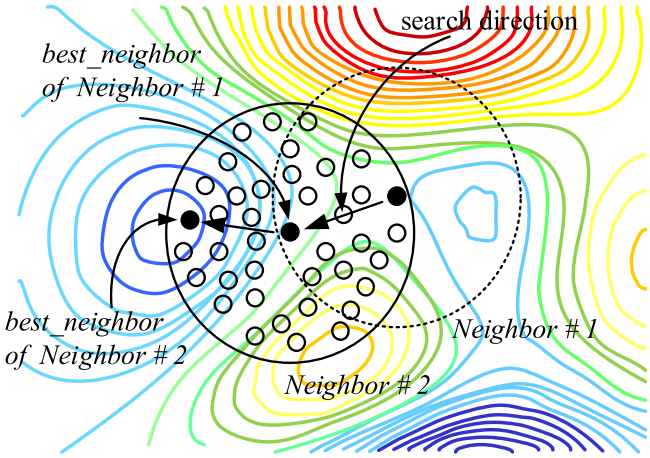

Fig. 11. Searching process in the next iteration.

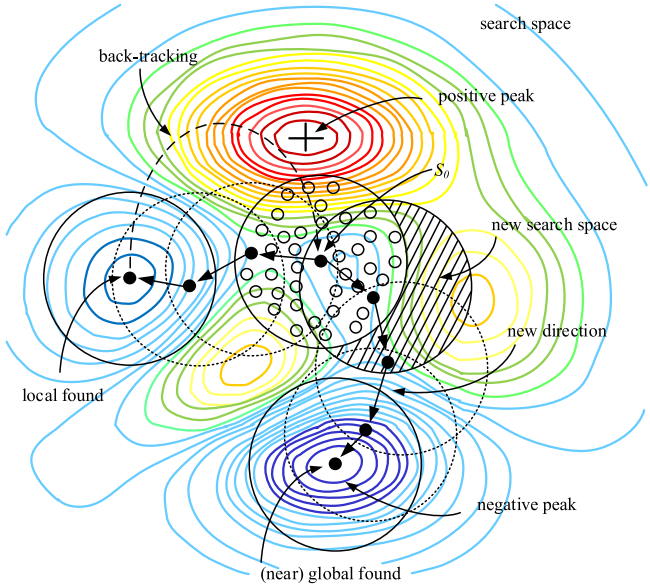

Fig. 12. Back-tracking in the ATS algorithm.

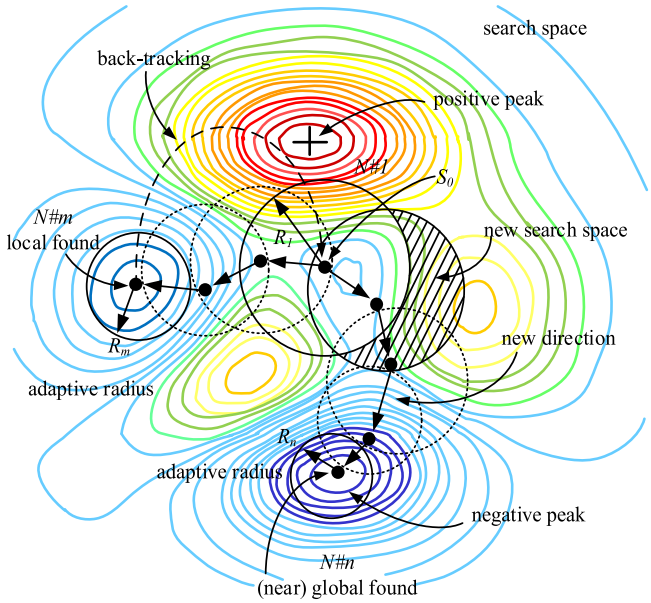

Fig. 13. ATS algorithm with adaptive search radius mechanism.

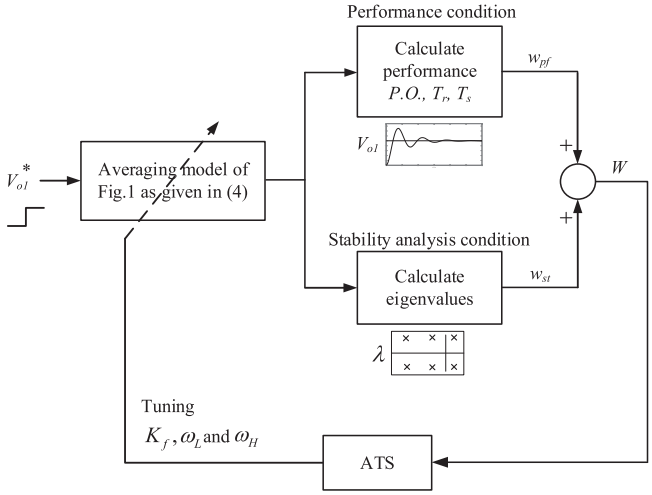

Fig. 14. Process diagram for the optimal feedforward loop design by the ATS.

Condition 4: Changing P_{CPL1} from 240 W to 300 W.

These conditions depend on the engineers. In this article, $P_{\mathrm{CPL}\,1}$ was set from 20 W to the rated power of the first buck converter, 300 W. The important criteria for setting P_{CPL1} is only that P_{CPL1} must be varied from the unstable point level to the rated power. The sampling power for setting the conditions can be defined arbitrarily.

Step 2: Evaluate the eigenvalues for each condition by the Jacobian matrix $\mathbf{A(x_o, u_o)}$ of the proposed model, as given in (4), with the system parameters given in the Appendix and the feedforward loop parameters from the ATS. The cost value for the stability condition (w_{st}) can be calculated by (6), which means that if the system is stable $\mathrm{Re}\{\lambda\} < 0$, w_{st} is set to 0. In contrast, if the system is unstable, w_{st} is set to a huge value

for the penalty condition, which is set to 10 000 here

$$\begin{aligned} &\text{if } \mathrm{Re}\{\lambda\} < 0 \\ &\quad w_{\mathrm{st}} = 0 \\ &\text{else} \\ &\quad w_{\mathrm{st}} = 10\,000 \\ &\text{end}. \end{aligned} \tag{6}$$

Step 3: Calculate the V_o response for each condition using the proposed model, as given in (4), with system parameters from the appendix and the feedforward loop parameters tuned from the ATS. The cost value for the performance condition (w_{pf}) can be calculated by

$$w_{pf} = \alpha\left(\frac{T_{r,\mathrm{ATS}}}{T_{r,\mathrm{CON}}}\right) + \beta\left(\frac{T_{s,\mathrm{ATS}}}{T_{s,\mathrm{CON}}}\right) + \gamma\left(\frac{\mathrm{P.O.}_{\mathrm{ATS}}}{\mathrm{P.O.}_{\mathrm{CON}}}\right) \tag{7}$$

where $T_{r,\mathrm{CON}}$, $T_{s,\mathrm{CON}}$, and $\mathrm{P.O.}_{\mathrm{CON}}$ are, respectively, the rise time, setting time, and percent overshoot of V_o response when the feedforward loop is designed by the conventional method under the same operating conditions with the ATS method. α, β, and γ are the priority coefficients of T_r, T_s, and P.O., respectively, in which the summation of these values must always be equal to 1. For design in this article, the values of α, β, and γ are set to 0.33, 0.33, and 0.34. This is because the $T_{r,\mathrm{ATS}}$, $T_{s,\mathrm{ATS}}$, and $\mathrm{P.O.}_{\mathrm{ATS}}$ are equally significant.

Step 4: In this article, the cost value for the optimal design (W) is expressed in (8), in which both the stability analysis and the output performance are considered. The ATS will tune the feedforward loop parameters K_f, ω_L, and ω_H until the optimal solution can be achieved (minimized W). The conditions used in the design were set from *Step 1*. Hence, n in (8) is set to four. The number of iterations is set to 100 as the termination criteria of each trial. As for the setting boundary, the setting methodology is based on the conventional design. The upper and lower limits of K_f, ω_L, and ω_H are set to [0.5, 5.0], [14.329 rad/s, 91.29 rad/s], and [286.57 rad/s, 1432.9 rad/s], respectively

$$W = \sum_{i=1}^{n} w_{pf,i} + w_{\mathrm{st},i}. \tag{8}$$

The resulting feedforward loop parameters, including their cost values represented by W, are given in Table I. It can be explicitly demonstrated from W that the ATS design method provides optimal output voltage performance compared with the conventional design method. To validate the proposed optimal design, a simulation using the MATLAB topology model and experimental results are presented in Section V.

V. Simulation and Experimental Validations

The proposed ATS design for the feedforward loop stabilization can provide the optimal output voltage response. Moreover, the system is always stable. In this section, the verification of the theoretical results by intensive time-domain simulation using MATLAB is reported alongside the detail of the experiment. The experimental rig of the considered ac–dc power system feeding two actively regulated buck converters is shown in Fig. 15.

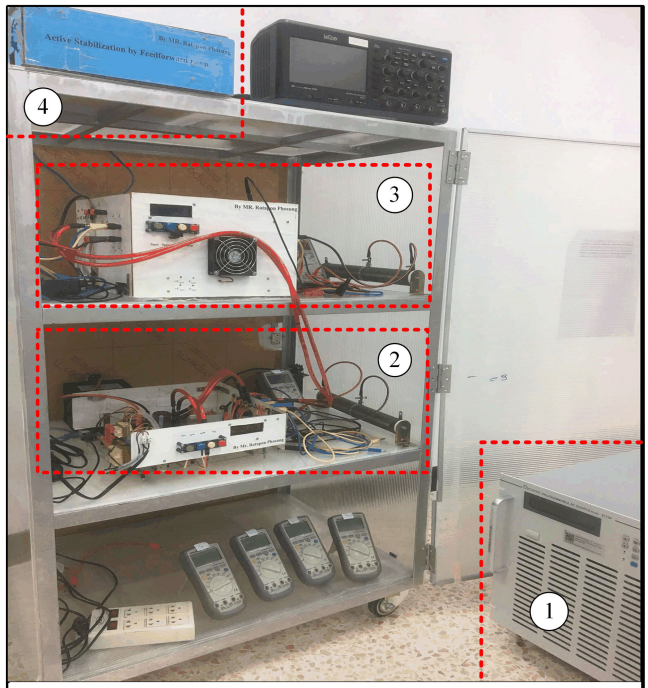

1. CHROMA programmable AC source
2. 6-Pulse Diode Rectifier & Controlled Buck Converter 2
3. Controlled Buck Converter 1
4. Active Stabilization Circuits by Feedforward Loop

Fig. 15. Schematic diagram of the experimental rig.

The three-phase ac distribution system was represented by a programmable ac source. The feedforward stabilizing loop was applied to only the first buck converter following the schematic diagram of Fig. 1.

The efficiency tests of the proposed feedforward loop designed by the ATS will consider two cases: The first case is that the system should be stable until the rated power can be achieved, and as for the second case, after applying the feedforward loop for instability mitigation, the load performance designed from the ATS must be better than those designed from the conventional approach. The resulting V_{dc} and V_{o1} waveforms (from simulation and experiment), using the proportional gain including the cutoff frequencies designed from both conventional and ATS methods for changing the total power level from 320 to 600 W, are illustrated in Fig. 16.

Fig. 16 confirms that the system always remains stable within the rated power, although the CPLs are continuously increased. This is indicated by the time-domain response of V_{dc} under various operating conditions. As for an output voltage regulation performance comparison, the details of the simulation and experiment in the zoomed area of Fig. 16 demonstrate that the ATS can provide optimal output performance. The performance comparison at the rated power is addressed in Table II from the simulation results and Table III from the experimental results. These tables present that ATS design can provide a significant improvement in terms of T_s and P.O. T_r, on the other hand, is slightly slower. However, the overall performance can be improved.

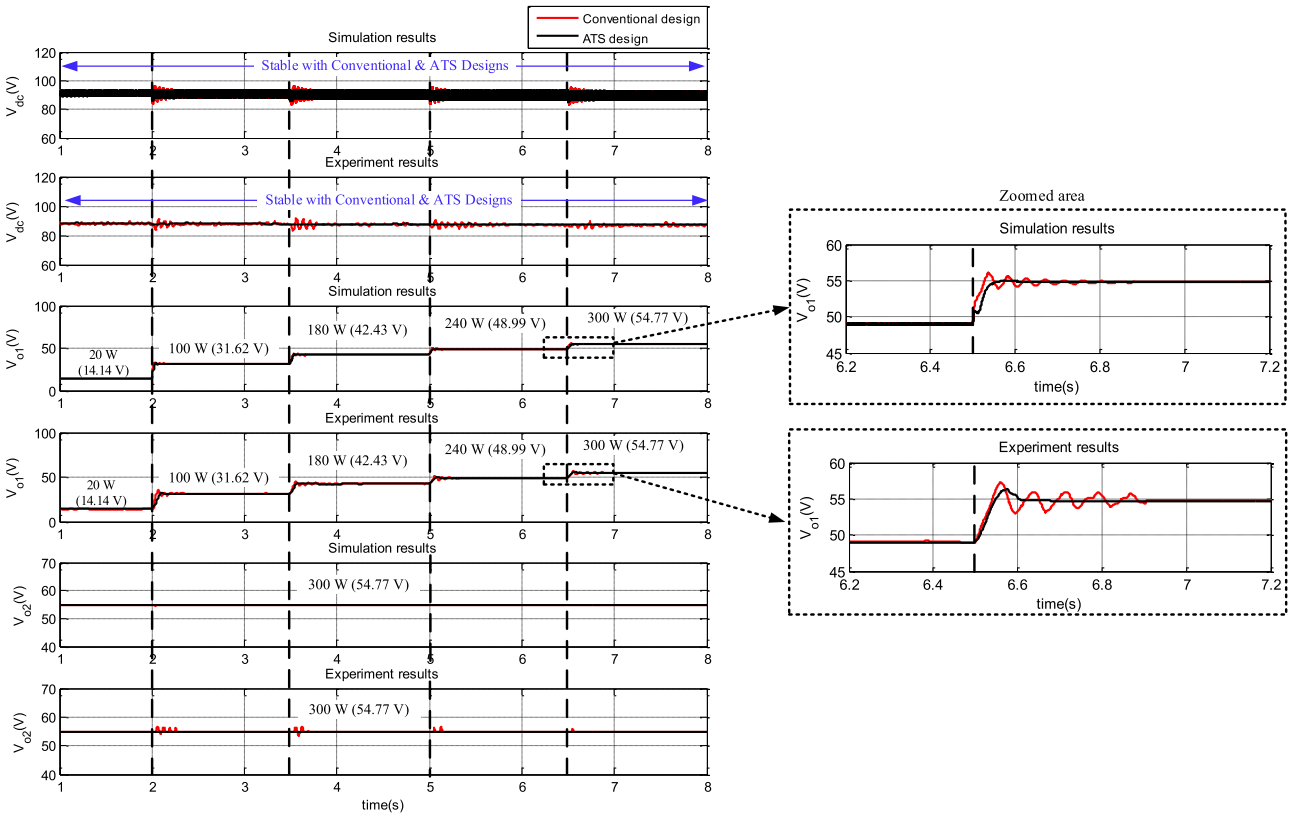

Fig. 16. AC–DC power system feeding paralleled controlled buck converters with active stabilization using a feedforward loop.

Overall, good agreement among analytical, simulation, and experimental results is confirmed. The system without the proposed stabilization becomes unstable when $P_{\mathrm{CPL,\ Total}}$ equals 320 W. After applying a feedforward loop that includes the ATS algorithm, the destabilizing effect can be eliminated to maintain stable operation and optimal load performance is achieved.

VI. Conclusion

In this article, the application of the ATS algorithm for active stabilization via a feedforward loop has been introduced. The new design technique has been used to eliminate the instability effect due to CPLs and to overcome the load performance effect when mitigation is applied to the load side. As a result, the proposed ac–dc power system remains stable until the rated power can be achieved. The load performance with mitigation designed from the ATS method is also better than that designed from the conventional method. Moreover, good agreement among theoretical, simulation, and experimental results has been achieved. Based on the proposed design technique, other AI techniques, such as the genetic algorithm, particle swarm optimization, etc., can be applied to design feedforward loop parameters instead of the ATS algorithm. Moreover, the analysis of the feedforward loop in this article is still useful even two or more variable power CPL is applied. If more CPL is applied, the mathematical model has derived again. After that, the new dynamic model can be used with the ATS algorithm following the process diagram of Fig. 14.

Appendix

The system parameters: $V_s = 40\ \mathrm{V_{rms/phase}}$, $\omega = 2\pi\times 50$ rad/s, $R_{\mathrm{eq}} = 0.0586\ \Omega$, $L_{\mathrm{eq}} = 248.73\ \mu$H, $C_{\mathrm{eq}} = 2$ nF, $r_L = 0.2756\ \Omega$, L_{dc} ($\Delta I_{\mathrm{dc}} \leq 0.6$ A) $= 39.0002$ mH, $r_c = 0.5280\ \Omega$, C_{dc} ($\Delta V_{\mathrm{dc}} \leq 0.26$ V) $= 1248.88\ \mu$F, $L_1 = L_2$ ($\Delta I_L \leq 0.2$ A) $=$ 15 mH, $C_1 = C_2$ ($\Delta V_C \leq 2.8$ mV) $= 1000\ \mu$F, $R_1 = R_2 = 10\ \Omega$, $A_{r,1} = A_{r,2} = 5$, $K_{pv,1} = K_{pv,2} = 0.1513$, $K_{pi,1} = K_{pi,2} =$ 15.7914, $K_{iv,1} = K_{iv,2} = 1.4102$, $K_{ii,1} = K_{ii,2} = 1265.8$, and $f_{sw,1} = f_{sw,2} = 10$ kHz.

References

[1] V. Grigore, J. Hatonen, J. Kyyra, and T. Suntio, "Dynamics of a buck converter with a constant power load," in *Proc. IEEE Power Electron. Spec. Conf.*, May 1998, pp. 72–78.

[2] A. B. Jusoh, "The instability effect of constant power loads," in *Proc. Nat. Power Energy Conf.*, Nov. 2004, pp. 175–179.

[3] C. H. Rivetta, A. Emadi, G. A. Williamson, R. Jayabalan, and B. Fahimi, "Analysis and control of a buck DC–DC converter operating with constant power load in sea and undersea vehicles," *IEEE Trans. Ind. Appl.*, vol. 42, no. 2, pp. 559–572, Mar./Apr. 2006.

[4] A. Emadi, A. Khaligh, C. H. Rivetta, and G. A. Williamson, "Constant power loads and negative impedance instability in automotive systems: Definition, modeling, stability, and control of power electronic converters and motor drives," *IEEE Trans. Veh. Technol.*, vol. 55, no. 4, pp. 1112–1125, Jul. 2006.

[5] A. M. Rahimi and A. Emadi, "An analytical investigation of DC/DC power electronic converters with constant power loads in vehicular power systems," *IEEE Trans. Veh. Technol.*, vol. 58, no. 6, pp. 2689–2702, Jul. 2009.

[6] S. Kim and S. S. Williamson, "Negative impedance instability compensation in more electric aircraft DC power systems using state space pole placement control," in *Proc. IEEE Veh. Power Propul. Conf.*, Sep. 2011, pp. 1–6.

[7] X. Feng, J. Liu, and F. C. Lee, "Impedance specifications for stable DC distributed power systems," *IEEE Trans. Power Electron.*, vol. 17, no. 2, pp. 157–162, Mar. 2002.
[8] A. Riccobono and E. Santi, "Comprehensive review of stability criteria for DC power distribution systems," *IEEE Trans. Ind. Appl.*, vol. 50, no. 5, pp. 3525–3535, Sep./Oct. 2014.
[9] K.-N. Areerak, T. Wu, S. V. Bozhko, G. M. Asher, and D. W. P. Thomas, "Aircraft power system stability study including effect of voltage control and actuators dynamic," *IEEE Trans. Aerosp. Electron. Syst.*, vol. 47, no. 7, pp. 2574–2589, Oct. 2011.
[10] K.-N. Areerak, S. V. Bozhko, G. M. Asher, L. De lillo, and D. W. P. Thomas, "Stability study for a hybrid AC-DC more-electric aircraft power system," *IEEE Trans. Aerosp. Electron. Syst.*, vol. 48, no. 1, pp. 329–347, Jan. 2012.
[11] J. Pakdeeto, K. Areerak, S. Bozhko, and K. Areerak, "Stabilization of DC microgrid systems using the loop-cancellation technique," *IEEE J. Emerg. Sel. Topics Power Electron.*, vol. 9, no. 3, pp. 2652–2663, Jun. 2021.
[12] M. Cespedes, L. Xing, and J. Sun, "Constant-power loads system stabilization by passive damping," *IEEE Trans. Power Electron.*, vol. 26, no. 7, pp. 1832–1836, Jul. 2011.
[13] X. Liu and S. Ma, "Large signal stabilization method of constant power loads by adding r parallel damping filters," in *Proc. IEEE Energy Convers. Congr. Expo.*, Sep. 2015, pp. 1314–1319.
[14] A. M. Rahimi and A. Emadi, "Active damping in dc/dc power electronic converters: A novel method to overcome the problems of constant power loads," *IEEE Trans. Ind. Electron.*, vol. 56, no. 5, pp. 1428–1439, Feb. 2009.
[15] P. Magne, D. Marx, B. Nahid-Mobarakeh, and S. Pierfederici, "Large-signal stabilization of a dc-link supplying a constant power load using a virtual capacitor: Impact on the domain of attraction," *IEEE Trans. Ind. Appl.*, vol. 48, no. 3, pp. 878–887, May/Jun. 2012.
[16] T. Sopapirm, K.-N. Areerak, and K.-L. Areerak, "The active damping stabilization of AC-DC power systems feeding constant power loads," *Int. Rev. Elect. Eng.*, vol. 12, no. 4, pp. 287–295, Jul./Aug. 2017.
[17] A. Khaligh, A. M. Rahimi, and A. Emadi, "Modified pulse-adjustment technique to control DC/DC converters driving variable constant-power loads," *IEEE Trans. Ind. Electron.*, vol. 55, no. 3, pp. 1133–1146, Mar. 2008.
[18] A. M. Rahimi, G. A. Williamson, and A. Emadi, "Loop-cancellation technique: A novel nonlinear feedback to overcome the destabilizing effect of constant-power loads," *IEEE Trans. Veh. Technol.*, vol. 59, no. 2, pp. 650–661, Feb. 2010.
[19] Y. Zhao, W. Qiao, and D. Ha, "A sliding-mode duty-ratio controller for dc/dc buck converters with constant power loads," *IEEE Trans. Ind. Appl.*, vol. 50, no. 2, pp. 1448–1458, Mar./Apr. 2014.
[20] M. Wu and D. D. Lu, "A novel stabilization method of LC input filter with constant power loads without load performance compromise in dc microgrid," *IEEE Trans. Ind. Electron.*, vol. 62, no. 7, pp. 4552–4562, Jul. 2015.
[21] A. Suyapan, K. Areerak, S. Bozhko, S. S. Yeoh, and K. Areerak, "Adaptive stabilization of a permanent magnet synchronous generator-based DC electrical power system in more electric aircraft," *IEEE Trans. Transp. Electrific.*, vol. 7, no. 4, pp. 2965–2975, Dec. 2021.
[22] M. Wu, D. D. C. Lu, and C. K. Tse, "Direct and optimal linear active methods for stabilization of LC input filters and DC/DC converters under voltage mode control," *IEEE J. Emerg. Sel. Topics Circuits Syst.*, vol. 5, no. 3, pp. 402–412, Sep. 2015.
[23] X. Zhang, Q.-C. Zhong, and W.-L. Ming, "Stabilization of a cascaded DC converter system via adding a virtual adaptive parallel impedance to the input of the load converter," *IEEE Trans. Power Electron.*, vol. 31, no. 3, pp. 1826–1832, Mar. 2016.
[24] X. Zhang, Q.-C. Zhong, and W.-L. Ming, "Stabilization of cascaded DC/DC converters via adaptive series-virtual-impedance control of the load converter," *IEEE Trans. Power Electron.*, vol. 31, no. 9, pp. 6057–6063, Sep. 2016.
[25] X. Zhang, Q.-C. Zhong, and W.-L. Ming, "A virtual RLC damper to stabilize DC/DC converters having an LC input filter while improving the filter performance," *IEEE Trans. Power Electron.*, vol. 31, no. 2, pp. 6057–6063, Dec. 2016.
[26] Y. Huangfu, S. Pang, B. Nahid-Mobarakeh, L. Guo, A. K. Rathore, and F. Gao, "Stability analysis and active stabilization of on-board DC power converter system with input filter," *IEEE Trans. Ind. Electron.*, vol. 65, no. 1, pp. 790–799, Jan. 2018.
[27] S. Pang *et al.*, "Interconnection and damping assignment passivity-based control applied to on-board DC–DC power converter system supplying constant power load," *IEEE Trans. Ind. Appl.*, vol. 55, no. 6, pp. 6476–6485, Nov. 2019.
[28] S. Pang, B. Nahid-Mobarakeh, S. Pierfederici, Y. Huangfu, G. Luo, and F. Gao, "Towards stabilization of constant power loads using IDA-PBC for cascaded LC filter DC/DC converters," *IEEE J. Emerg. Sel. Topics Power Electron.*, vol. 9, no. 2, pp. 1302–1314, Apr. 2021.
[29] R. Roy and S. Kapat, "Input filter-based ripple injection for mitigating limit cycling in buck converters driving CPL," *IEEE J. Emerg. Sel. Topics Power Electron.*, vol. 9, no. 2, pp. 1315–1327, Apr. 2021.
[30] O. Pizniur, Z. Shan, and J. Jatskevich, "Ensuring dynamic stability of constant power loads in dc telecom power systems and data centers using active damping," in *Proc. IEEE Int. Telecommun. Energy Conf .*, Sep./Oct. 2014, pp. 1–8.
[31] K. Areerak, T. Sopapirm, S. Bozhko, C. I. Hill, A. Suyapan, and K. Areerak, "Adaptive stabilization of uncontrolled rectifier based AC–DC power systems feeding constant power loads," *IEEE Trans. Power Electron*, vol. 33, no. 10, pp. 8927–8935, Oct. 2018.
[32] M. Wu and D. D. C. Lu, "Investigation on active method for stabilization of LC input filter and DC/DC buck converter under voltage mode control," in *Proc. IEEE Int. Conf. Power Electron. Drive Syst.*, 2015, pp. 721–726.
[33] D. Puangdownreong, K.-N. Areerak, S. Sujitjorn, and T. Kulworawanichpong, "Convergence analysis of adaptive tabu search," *Int. J. Sci. Asia*, vol. 30, no. 2, pp. 183–190, Jul. 2009.
[34] T. Sopaprim, K.-N. Areerak, and K.-L. Areerak, "The identification of AC-DC power system parameter using an adaptive tabu search technique," *Int. Rev. Elect. Eng.*, vol. 7, no. 4, pp. 4655–4662, Jul./Aug. 2012.
[35] P. Ruttanee, K. Areerak, and K. Areerak, "An artificial intelligence based system identification of AC-DC power system including a three- phase controlled rectifier," *Int. J. Control Automat.*, vol. 7, no. 12, pp. 199–218, Dec. 2014.
[36] J. Pakdeeto, R. Chanpittayagit, K. Areerak, and K. Areerak, "The optimal controller design of buck-boost converter by using adaptive tabu search algorithm based on state-space averaging model," *J. Elect. Eng. Technol.*, vol. 12, no. 3, pp. 1146–1155, Jan. 2017.
[37] A. Emadi, "Modeling of power electronic loads in AC distribution systems using the generalized state-space averaging method," *IEEE Trans. Ind. Electron.*, vol. 51, no. 5, pp. 992–1000, Oct. 2004.
[38] T. Sopapirm, K.-N. Areerak, and K.-L. Areerak, "Stability analysis of AC distribution system with six-pulse diode rectifier and multi-converter power electronic loads," *Int. Rev. Elect. Eng.*, vol. 6, no. 7, pp. 2919–2928, Nov./Dec. 2011.
[39] J. Pakdeeto, K.-N. Areerak, and K.-L. Areerak, "Modelling and stability analysis of AC-DC power systems feeding a speed controlled DC motor," *J. Elect. Eng. Technol.*, vol. 13, no. 4, pp. 1566–1577, Jul. 2018.

Ratapon Phosung was born in Ang Thong, Thailand, in 1996. He received the B.Eng. (First class honors) and M.Eng. degrees in electrical engineering from the Suranaree University of Technology (SUT), Nakhon Ratchasima, Thailand, in 2018 and 2021, respectively.

In 2021, he was a Researcher with the Institute of Research and Development, SUT. His main research interests include system identifications, artificial intelligence applications, stability analysis of power systems with constant power loads, modeling and control of power electronic-based systems, and control theory.

Kongpan Areerak (Member, IEEE) received the B.Eng. and M.Eng. degrees from the Suranaree University of Technology (SUT), Nakhon Ratchasima, Thailand, in 2000 and 2001, respectively, and the Ph.D. degree from the University of Nottingham, Nottingham, U.K., in 2009, all in electrical engineering.

In 2002, he was a Lecturer with the Electrical and Electronic Department, Rangsit University, Lak Hok, Thailand. Since 2003, he has been a Lecturer with the School of Electrical Engineering, SUT, where he became an Associate Professor of electrical engineering in 2015. His main research interests include system identifications, artificial intelligence applications, stability analysis of power systems with constant power loads, modeling and control of power electronic-based systems, and control theory.

Theppanom Sopapirm received the B.Eng., M.Eng., and Ph.D. degrees in electrical engineering from the Suranaree University of Technology, Nakhon Ratchasima, Thailand, in 2009, 2011, and 2017, respectively.

Since 2016, he has been a Lecturer with the Department of Electrical Power Engineering, Mahanakorn University of Technology, Bangkok, Thailand. His research interests include stability analysis, modeling of power electronic systems, digital control, FPGA, and AI applications.

Kongpol Areerak (Member, IEEE) received the B.Eng., M.Eng., and Ph.D. degrees in electrical engineering from the Suranaree University of Technology (SUT), Nakhon Ratchasima, Thailand, in 2000, 2003, and 2007, respectively.

Since 2007, he has been a Lecturer and the Head of Power Quality Research Unit (PQRU), School of Electrical Engineering, SUT, where he became an Associate Professor of electrical engineering in 2015. His main research interests include active power filter, harmonic elimination, motor drives, AI applications, and intelligence control systems.